

Article

Flat-Top Focal Spot and Polarization Conversion Obtained in Tightly Focused Circularly Polarized Light

Sergey S. Stafeev ^{1,2}, Vladislav D. Zaitsev ^{1,2,*} and Victor V. Kotlyar ^{1,2}

¹ IPSI RAS—Branch of the FSRC “Crystallography and Photonics” RAS, Molodogvardeyskaya 151, 443001 Samara, Russia

² Department of Technical Cybernetics, Samara National Research University, Moskovskoye Shosse 34, 443086 Samara, Russia

* Correspondence: zaitsev-vlad@yandex.ru

Abstract: In this paper, using the Richards–Wolf equations, the focusing of circularly polarized light with flat diffractive lenses is considered. It is shown that, as the numerical aperture (NA) of the lens increases, the size of the focal spot first decreases and then begins to grow. The minimum focal spot is observed at $NA = 0.96$ ($FWHM = 0.55 \lambda$). With a further increase in the numerical aperture of the lens, the growth of the longitudinal component leads to an increase in the size of the focal spot. When a flat diffractive lens is replaced by an aplanatic lens, the size of the focal spot decreases monotonically as the numerical aperture of the lens increases. In this case, the minimum focal spot will be $FWHM = 0.58 \lambda$ and, with a larger numerical aperture, $NA = 0.99$. We also reveal that, at the focus of a circularly polarized laser beam, different radius circles are observed to be centered on the optical axis, where polarization vectors rotate oppositely (clockwise and anticlockwise). This phenomenon of radius-dependent ‘spin’ separation may be interpreted as a manifestation of the radial spin Hall effect at the focus.

Keywords: tight focusing; Richards–Wolf formula; optical vortex; polarization conversion

1. Introduction

Tight focusing attracts the attention of researchers due to various effects that do not appear (or are weakly pronounced) when light is focused with lenses with small numerical apertures. For example, in complex patterns of transverse energy fluxes [1–4], polarization conversion [5–7] can be observed at the focus, and, when considering the intensity at the focus, one can observe focal spots of various shapes [8–10], in particular, spots with a flat top (flat-top focus) [11–13]. In such focal spots, the shape of the spot approaches a super-Gaussian distribution. Flat-top beams are needed in lithography [14,15] or optical data transmission through the atmosphere [16].

In this paper, using the Richards–Wolf equations, the focusing of light with circular polarization with flat diffractive lenses is investigated. It is shown that, as the numerical aperture of the lens increases, the size of the focal spot first decreases and then begins to grow. The minimum focal spot is observed at $NA = 0.96$ ($FWHM = 0.55 \lambda$). With a further increase in the numerical aperture of the lens, the growth of the longitudinal component leads to an increase in the size of the focal spot. When a flat diffractive lens is replaced by an aplanatic lens, the size of the focal spot decreases monotonically as the numerical aperture of the lens increases.



Citation: Stafeev, S.S.; Zaitsev, V.D.; Kotlyar, V.V. Flat-Top Focal Spot and Polarization Conversion Obtained in Tightly Focused Circularly Polarized Light. *Photonics* **2023**, *10*, 32. <https://doi.org/10.3390/photonics10010032>

Received: 7 November 2022

Revised: 5 December 2022

Accepted: 23 December 2022

Published: 28 December 2022



Copyright: © 2022 by the authors. Licensee MDPI, Basel, Switzerland. This article is an open access article distributed under the terms and conditions of the Creative Commons Attribution (CC BY) license (<https://creativecommons.org/licenses/by/4.0/>).

2. Methods

A field near the sharp focus can be described using the Richards–Wolf integrals [5] (Figure 1):

$$\mathbf{U}(\rho, \psi, z) = -\frac{if}{\lambda} \int_0^{\theta_0} \int_0^{2\pi} B(\theta, \varphi) T(\theta) \mathbf{P}(\theta, \varphi) \times \exp\{ik[\rho \sin \theta \cos(\varphi - \psi) + z \cos \theta]\} \sin \theta \, d\theta \, d\varphi, \quad (1)$$

where $\mathbf{U}(\rho, \psi, z)$ is the electric or magnetic field strength, $B(\theta, \varphi)$ is the amplitude of the electric or magnetic field in the exit pupil of a wide-aperture optical system (θ is the polar angle, φ is the azimuthal angle), $T(\theta)$ is lens' apodization function, f is the focal length, $k = 2\pi/\lambda$ is the wavenumber, λ is the wavelength of light (assumed to be 532 nm in the numerical simulation), θ_0 is the maximum polar angle determined by the numerical aperture of the lens ($NA = \sin \theta_0$), and $\mathbf{P}(\theta, \varphi)$ is the polarization vector, for the electric and magnetic field strength having the form:

$$\mathbf{P}(\theta, \varphi) = \begin{bmatrix} 1 + \cos^2 \varphi (\cos \theta - 1) \\ \sin \varphi \cos \varphi (\cos \theta - 1) \\ -\sin \theta \cos \varphi \end{bmatrix} a(\theta, \varphi) \begin{bmatrix} \sin \varphi \cos \varphi (\cos \theta - 1) \\ 1 + \sin^2 \varphi (\cos \theta - 1) \\ -\sin \theta \sin \varphi \end{bmatrix} b(\theta, \varphi), \quad (2)$$

where $a(\theta, \varphi)$ and $b(\theta, \varphi)$ are functions describing the polarization state of the x - and y -components of the electric field strength at the focus.

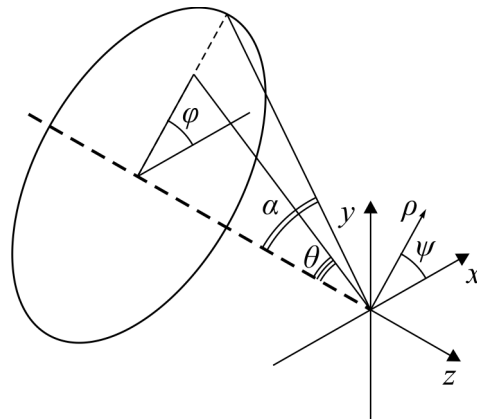


Figure 1. The geometric interpretation of the problem.

Since the intensity and the on-axis energy flow for light with left- and right-hand circular polarization are the same, we only consider the right-hand polarization of the field, the Jones vector for which has the form:

$$\mathbf{E}_R = \begin{pmatrix} a(\theta, \varphi) \\ b(\theta, \varphi) \end{pmatrix} = \frac{A(\theta)}{\sqrt{2}} \begin{pmatrix} 1 \\ i \end{pmatrix} \quad (3)$$

where $A(\theta)$ is the initial field amplitude, depending only on the polar angle.

Projections of the electric field strength vector near the focus for the initial field (3) have the form [17]:

$$\begin{aligned} E_{x,R} &= \frac{-i}{\sqrt{2}} (I_{0,0} + e^{2i\varphi} I_{2,2}), \\ E_{y,R} &= \frac{1}{\sqrt{2}} (I_{0,0} - e^{2i\varphi} I_{2,2}), \\ E_{z,R} &= -\sqrt{2} e^{i\varphi} I_{1,1}. \end{aligned} \quad (4)$$

where

$$I_{\nu,\mu} = \left(\frac{4\pi f}{\lambda}\right) \int_0^{\theta_0} \sin^{\nu+1}\left(\frac{\theta}{2}\right) \cos^{3-\nu}\left(\frac{\theta}{2}\right) T(\theta) A(\theta) e^{ikz \cos \theta} J_{\mu}(\xi) d\theta, \quad (5)$$

where $\xi = krsin\theta$, $J_\mu(\xi)$ is the first-kind Bessel function.

Equation (4) shows that individual transverse intensity components $I_x = |E_{x,R}|^2$ and $I_y = |E_{y,R}|^2$ are non-zero on the optical axis ($I_{0,0}(r = 0) > 0$) and are not symmetric relative to the azimuthal angle ϕ , while the longitudinal intensity component $I_z = |E_{z,R}|^2$ has the form of a symmetrical ring with zero at $r = 0$.

The initial amplitude function $A(\theta)$ (assumed to be real) can be a constant (plane wave) or in the form of a Gaussian beam

$$A(\theta) = \exp\left(\frac{-\gamma^2 \sin^2 \theta}{\sin^2 \theta_0}\right) \tag{6}$$

where γ is a constant.

From (4), we can obtain the intensity distribution at the focus for the initial field (3):

$$I_R(r, z = 0) = I_x + I_y + I_z = I_{0,0}^2 + I_{2,2}^2 + 2I_{1,1}^2. \tag{7}$$

It can be seen from (7) that the focal spot from a circularly polarized beam (3) has a round shape, as the intensity distribution (7) depends only on the radial variable r .

Previously, in [13], the focusing of radially polarized light was considered and the obtaining of a flat-top focus due to the redistribution of energy between the transverse and longitudinal components was demonstrated. Equation (7) shows that the same approach can be applied to circular polarization.

Let us also consider the behavior of polarization in the vicinity of the sharp focus for this case. Previously, in [18], we showed that, when sharply focusing linearly polarized light, regions arise in which the polarization becomes elliptical at a near-wavelength distance from the focal plane. Directly in the focal plane at $z = 0$, the polarization remains linear. The polarization state can be characterized by the Stokes vector or the spin angular momentum. The presence of circular polarization in the beam cross-section is shown by the third component of the Stokes vector s_3 or the longitudinal component SAM_z of the spin angular momentum (SAM), and they are equal to each other and are equal to:

$$SAM_z = s_3 = 2\text{Im}(E_x^* E_y) \tag{8}$$

Using Formula (4), we can show that, directly at the focus:

$$SAM_z = I_{0,0}^2 - I_{2,2}^2 \tag{9}$$

Equation (9) shows that there are regions where the longitudinal component of the spin angular momentum changes sign. Near the optical axis, it is positive, since $I_{0,0}^2 > I_{2,2}^2$. Moreover, on a circle of a certain radius, when the condition is satisfied $I_{0,0}^2 < I_{2,2}^2$, the longitudinal component of the spin density vector becomes negative. Thus, in the focal plane, a change in the direction of the rotation of circular polarization should be observed; moreover, near the optical axis, the initial right-hand circular polarization (3) remains, and, at some distance from the optical axis, a light ring with left-hand circular polarization appears. This effect can be called the radial spin Hall effect, since light with a different spin sign at the focus takes place on different light rings with the same center on the optical axis.

We also note that, at some distance from the focal plane, we can assume that $e^{ikz \cos \theta} \approx 1 + ikz \cos \theta$; then, Equation (5) can be represented as

$$I_{\nu,\mu} = Ir_{\nu,\mu} + ikz Ii_{\nu,\mu} \tag{10}$$

where

$$Ir_{\nu,\mu} = \left(\frac{4\pi f}{\lambda}\right) \int_0^{\theta_0} \sin^{\nu+1}\left(\frac{\theta}{2}\right) \cos^{3-\nu}\left(\frac{\theta}{2}\right) T(\theta) A(\theta) J_\mu(\xi) d\theta, \tag{11}$$

$$I_{i_{\nu,\mu}} = \left(\frac{4\pi f}{\lambda}\right) \int_0^{\theta_0} \sin^{\nu+1}\left(\frac{\theta}{2}\right) \cos^{3-\nu}\left(\frac{\theta}{2}\right) T(\theta) A(\theta) \cos\theta J_{\mu}(\zeta) d\theta. \tag{12}$$

Then, instead of (9), we can write:

$$SAM_z = (I_{r_{0,0}}^2 - I_{r_{2,2}}^2) + (kz)^2 (I_{i_{0,0}}^2 - I_{i_{2,2}}^2). \tag{13}$$

Equation (13) shows that, in contrast to [18], before and after the focus, the SAM pattern is the same, and differs from the distribution at the focus only in one thing: the first light ring with the negative SAM ($SAM_z < 0$) has a larger radius than at the focus.

3. Results

3.1. Numerical Simulation of Light Focusing by a Planar Diffractive Lens

Using Formula (1), we numerically model the focusing of a circularly polarized laser beam (3) with a flat diffractive lens, with its apodization function given by $T(\theta) = \cos^{-3/2}\theta$. We assume focusing a plane wave $A(\theta) = 1$ of wavelength $\lambda = 532$ nm. Previously, analyzing the sharp focusing of laser beams, researchers noted that it is with the help of flat diffractive lenses that it is possible to obtain a focal spot with smaller focus sizes than when focusing with an aplanatic lens [19].

Figure 2 shows a change in the focal spot diameter along the full width at half maximum with increasing numerical aperture of the lens.

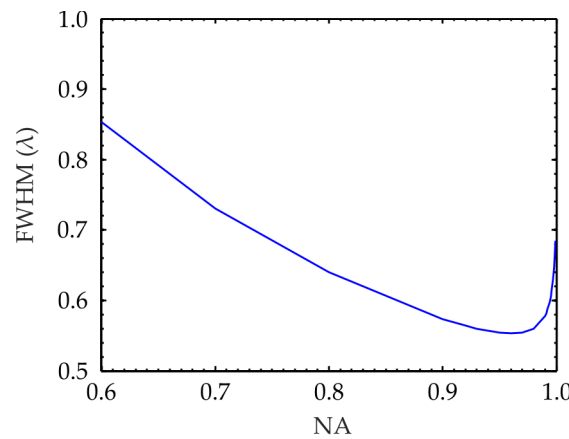


Figure 2. Dependence of the focal spot diameter on the full width at half maximum on the numerical aperture of the flat diffractive lens in the focusing of a plane wave with circular polarization.

Figure 2 shows that, as the numerical aperture of the lens increases, the size of the focal spot first decreases and then begins to grow. The minimum focal spot is observed at $NA = 0.96$ and the spot diameter at the full width at half maximum is $FWHM = 0.55 \lambda$.

The increase in the size of the focal spot is explained by the redistribution of energy between the transverse and longitudinal components of the intensity in such a way that the ring-shaped longitudinal component increases, broadening the spot. For clarity, Figures 3 and 4 show the distribution of intensity and its individual components for numerical apertures equal to 0.8 (Figure 3) and 0.999 (Figure 4).

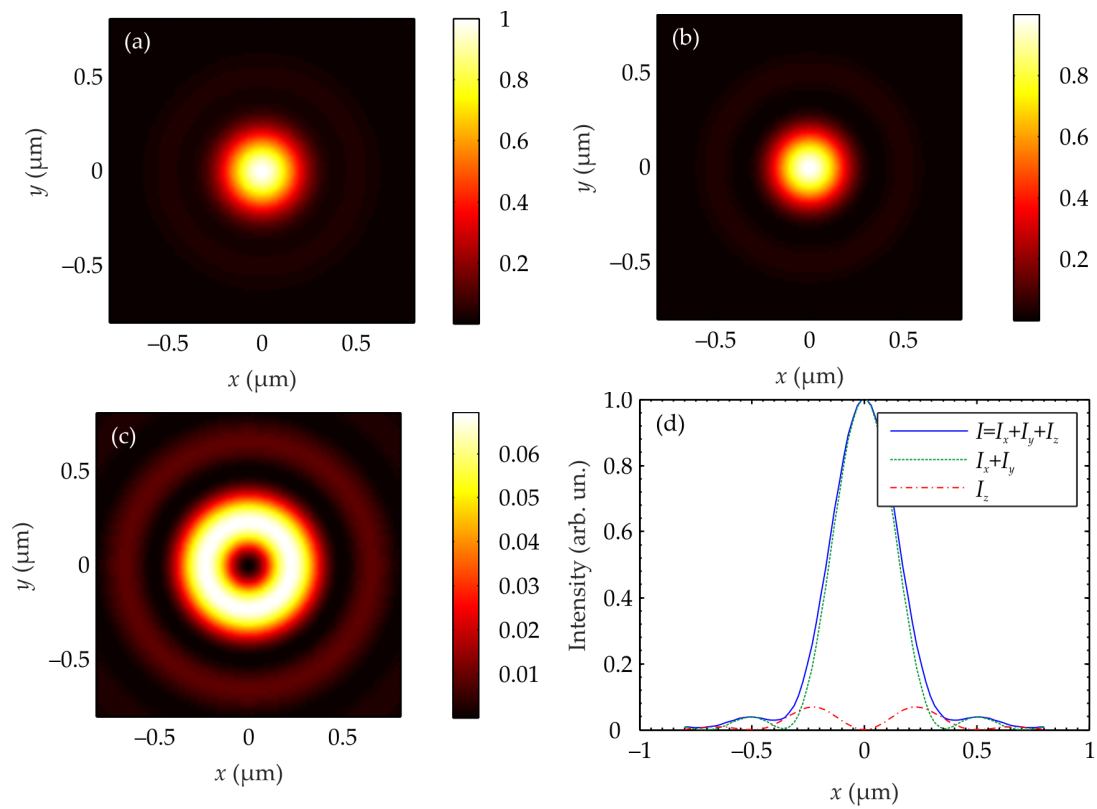


Figure 3. Distributions of intensity at the focus (a) and intensity components I_r (b) and I_z (c) when focusing light with a flat diffractive lens with NA = 0.8. The intensity profile along the x -axis (d).

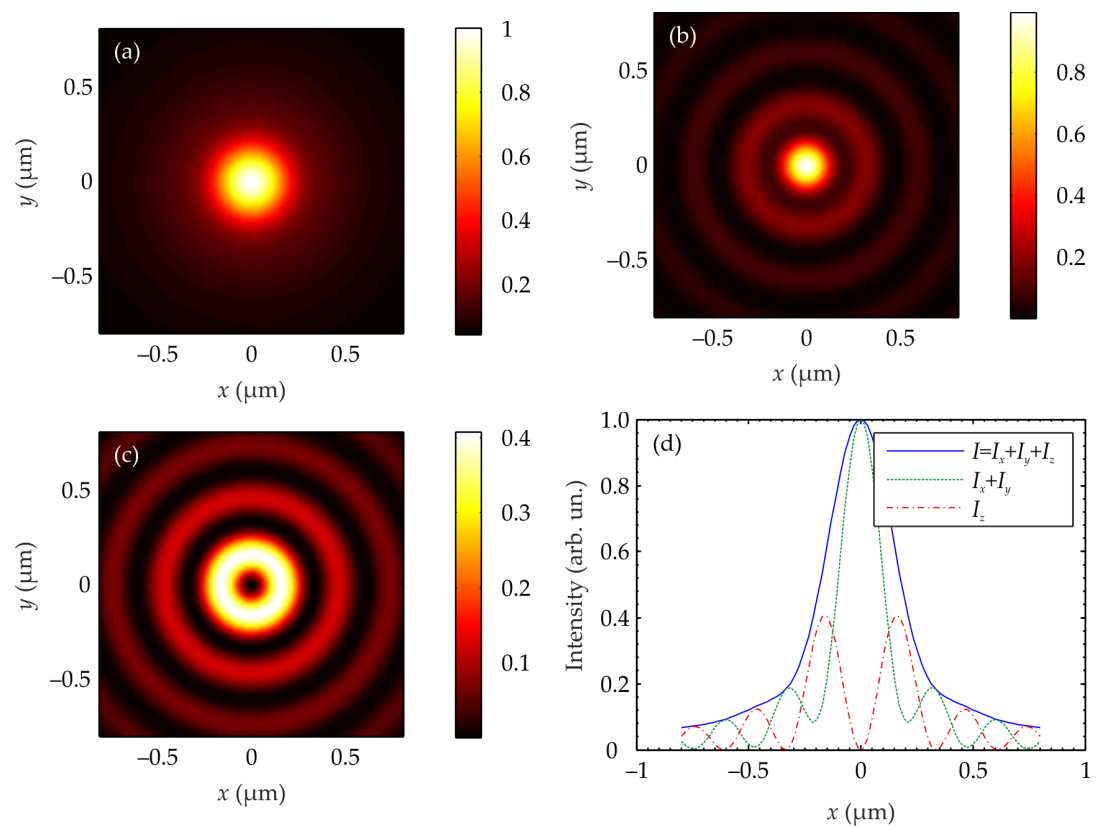


Figure 4. Distributions of intensity at the focus (a) and intensity components I_r (b) and I_z (c) when focusing light with a flat diffractive lens with NA = 0.999. The intensity profile along the x -axis (d).

3.2. Numerical Simulation of Light Focusing with an Aplanatic Lens

Let us replace the flat diffractive lens with an aplanatic lens whose apodization function has the form $T(\theta) = \cos^{1/2}\theta$. Figure 5 shows a change in the focal spot diameter in terms of the intensity at full width at half maximum with increasing numerical aperture of the lens.

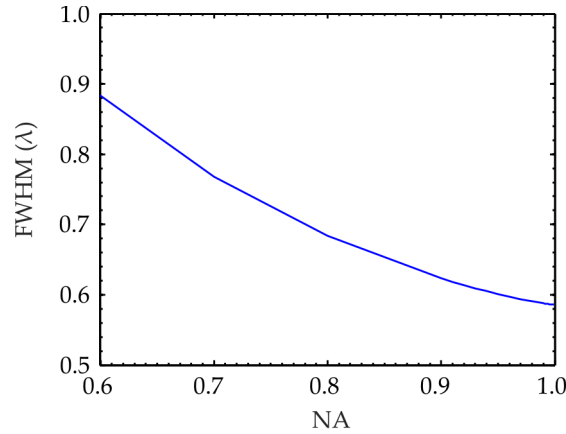


Figure 5. Diameter of the focal spot at full width at half maximum of the intensity vs. the lens numerical aperture when focusing a circularly polarized plane wave.

Figure 5 shows that, unlike a flat diffractive lens, an aplanatic lens does not have an inflection point, and the size of the focal spot decreases monotonically with the increasing numerical aperture of the lens.

For example, Figure 6 shows the distributions of the intensity and its individual components at the focus. In this case ($NA = 0.95$), we see that the focal spot size is $FWHM = 0.60 \lambda$, which agrees well with results reported in [20], where it was shown that circularly and linearly polarized incident beams were produced at the tight focus identical circular symmetric distributions of an on-axis energy flow (other conditions being the same). From Figure 6, it can be seen that the longitudinal component of the intensity is small in this case.

Thus, comparing the focusing of a Gaussian beam (6) with circular polarization using a diffractive lens (Figure 2) and a refractive lens (Figure 5), it can be argued that the minimum focal spot size for a diffractive lens is $FWHM = 0.55 \lambda$ and is achieved with a numerical aperture $NA = 0.96$, and the minimum focal spot size for an aplanatic lens is larger and equals $FWHM = 0.58 \lambda$ for a numerical aperture $NA \approx 1$.

3.3. Polarization near the Sharp Focus

Let us now consider the change of polarization when sharply focusing a light field circularly polarized in the source plane. The state of polarization is characterized by the third component of the normalized Stokes vector:

$$\begin{aligned}
 S_1 &= \frac{s_1}{s_0} = \frac{E_x E_x^* - E_y E_y^*}{E_x E_x^* + E_y E_y^*}, \\
 S_2 &= \frac{s_2}{s_0} = \frac{2\text{Re}(E_x^* E_y)}{E_x E_x^* + E_y E_y^*}, \\
 S_3 &= \frac{s_3}{s_0} = \frac{S_{AM_z}}{s_0} = \frac{2\text{Im}(E_x^* E_y)}{E_x E_x^* + E_y E_y^*}
 \end{aligned} \tag{14}$$

We recall that circular polarization corresponds to $S_3 = \pm 1$.

Figure 7 shows the distribution of three components of the normalized Stokes vector in the focal plane, and Figure 8 shows the distribution of three components of the normalized Stokes vector in a plane located at a distance $z = \lambda$ from the focus.

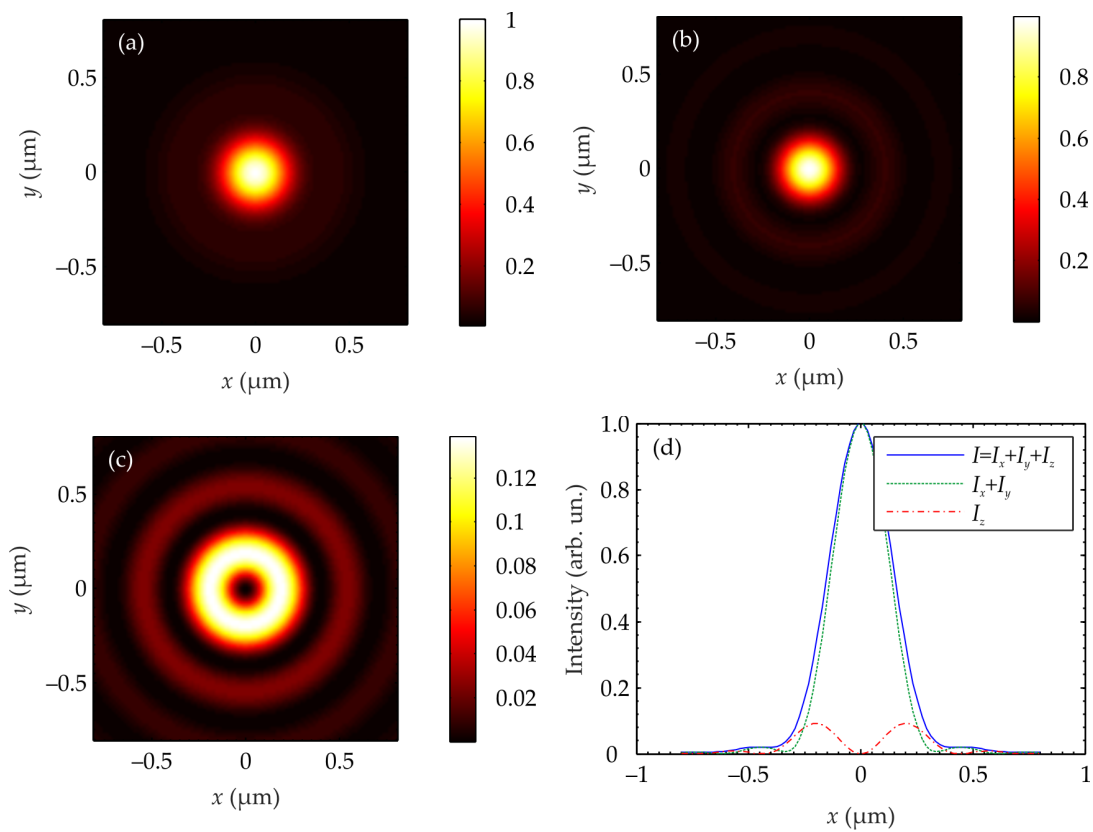


Figure 6. Distributions of intensity at the focus (a) and intensity components I_r (b) and I_z (c) when focusing light with an aplanatic lens with NA = 0.95. The intensity profile along x -axis (d).

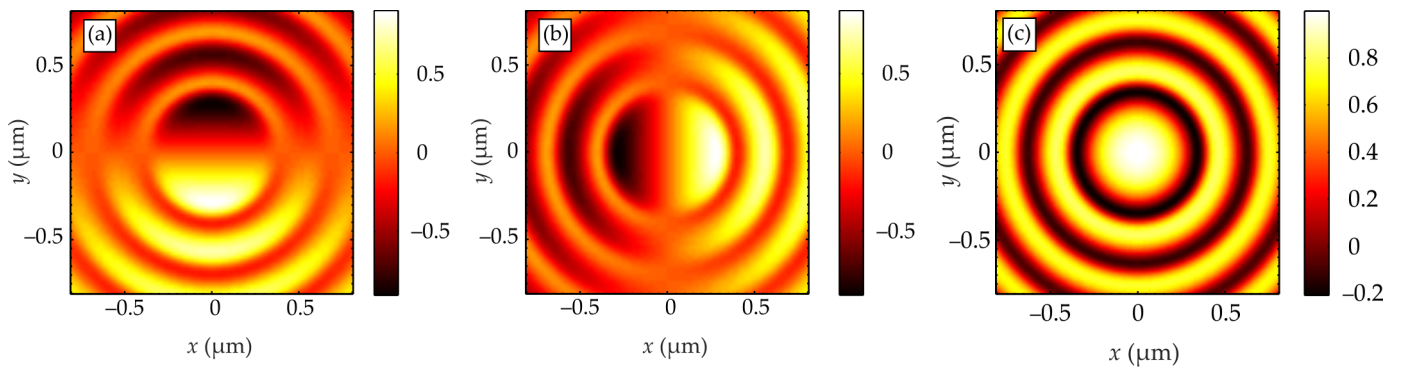


Figure 7. Distribution of the three components of the normalized Stokes vector S_1 (a), S_2 (b), S_3 (c) in the focal plane when focusing light with an aplanatic lens with NA = 0.95.

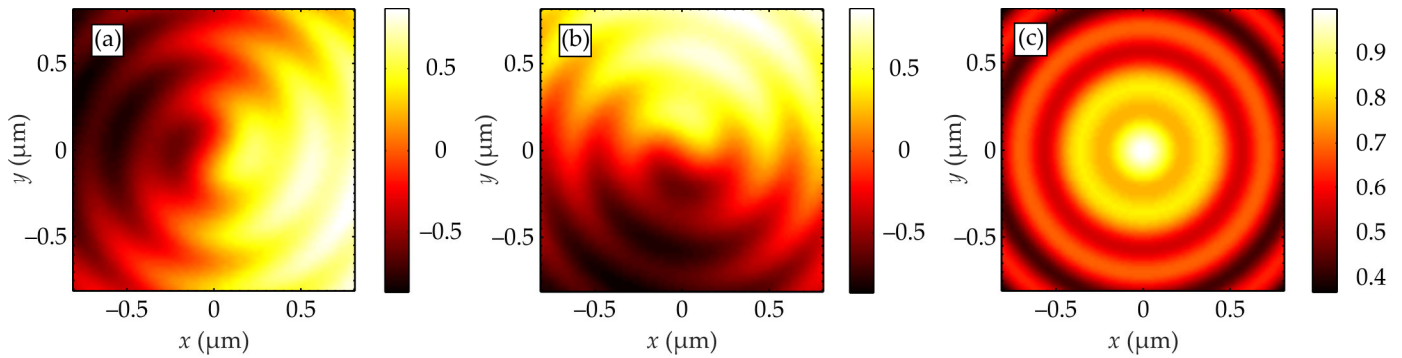


Figure 8. Distribution of the three components of the normalized Stokes vector S_1 (a), S_2 (b), S_3 (c) in a plane located at a distance $z = \lambda$ from the focus when light is focused by an aplanatic lens with $NA = 0.95$.

3.4. Focusing Optical Vortex with Circular Polarization

Consider further the focusing of an optical vortex with circular polarization:

$$\mathbf{E}_R = \begin{pmatrix} a(\theta, \varphi) \\ b(\theta, \varphi) \end{pmatrix} = \frac{A(\theta)e^{im\varphi}}{\sqrt{2}} \begin{pmatrix} 1 \\ i \end{pmatrix} \quad (15)$$

where m is the topological charge of the vortex. We note that the function $A(\theta)$ in (15) is identical to that entering Equation (3) and is a Gaussian function defined in (6). Previously, it has been shown [21] that, when focusing circularly polarized optical vortices with a planar diffractive lens, negative values of the longitudinal Poynting vector component can be observed at the focus, meaning that a reverse energy flow occurs. At $m = -1$, a peak intensity distribution is observed at the focus [21]. In this case, the distribution of the transverse intensity component has the form of a ring, while the distribution of the longitudinal component has the form of a central peak. Actually, using a method discussed in [17], projections of the electric field (15) analogous to Equation (4) can be derived at the focus:

$$\begin{aligned} E_x &= \frac{i^{m-1}}{\sqrt{2}} e^{im\varphi} (I_{0,m} + e^{2i\varphi} I_{2,m+2}), \\ E_y &= \frac{i^m}{\sqrt{2}} e^{im\varphi} (I_{0,m} - e^{2i\varphi} I_{2,m+2}), \\ E_z &= -\sqrt{2} i^m e^{i(m+1)\varphi} I_{1,m+1}. \end{aligned} \quad (16)$$

From (16), the relation for the intensity distribution at the focus takes the form:

$$I_V(r, z = 0) = I_{0,m}^2 + I_{2,m+2}^2 + 2I_{1,m+1}^2. \quad (17)$$

For an optical vortex with topological charge $m = -1$, Equation (17) is rearranged to

$$I_{V,-1}(r, z = 0) = I_{0,1}^2 + I_{2,1}^2 + 2I_{1,0}^2. \quad (18)$$

An analysis of (18) suggests that, on the optical axis, only the third term is non-zero because the integral $I_{1,0}$ in Equation (5) contains a zero-order Bessel function that equals unity at zero-valued argument: $J_0(0) = 1$. That is why, at the focus, and given $m = -1$, the transverse intensity of field (15), $I_{0,1}^2 + I_{2,1}^2$, is shaped as a ring with an on-axis intensity null, whereas the longitudinal intensity $2I_{1,0}^2$ is in the form of a circular spot with the on-axis maximum.

Similar to Equation (9) for the SAM at the focus of the light field (3), the SAM at the focus field (15) can be derived from Equation (13):

$$SAM_z = I_{0,1}^2 - I_{2,1}^2 \quad (19)$$

Equation (19) suggests that, although the intensity (18) on the optical axis is nonzero, SAM_z takes a zero value. The reason for this is that the on-axis intensity is contributed to by a light field with the on-axis polarization vector, which does not contribute to the SAM_z . At $r > 0$, if $I_{0,1}^2 > I_{2,1}^2$, then $SAM_z > 0$ (polarization vector rotates anticlockwise); moreover, if $I_{0,1}^2 < I_{2,1}^2$, then $SAM_z < 0$ (polarization vector rotates clockwise). Hence, we conclude that, similar to field (9), a radial spin Hall effect occurs at the focus for vortex field (15).

The dependence of the focal spot diameter on the numerical aperture of a flat diffractive lens is shown in Figure 9.

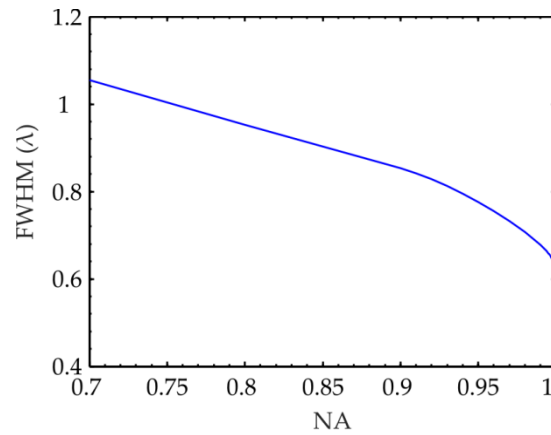


Figure 9. Focal spot diameter at full width at half maximum when focusing an optical vortex ($m = -1$) with circular polarization when focusing with a flat diffractive lens.

When the numerical aperture of the lens is approximately equal to $NA = 0.93$, a flat top is observed at the formed focus (Figure 10), and the focal spot diameter for this case is $FWHM = 1.03 \lambda$.

Meanwhile, Figure 9 depicts a flat-top focal intensity pattern produced with the aid of a planar diffractive lens, and we note that the use of a convenient aplanatic lens would also have resulted in a similarly shaped flat-top focal spot. The fact is that a flat-top focus can be attained when focusing a circularly polarized optical vortex and not a circularly polarized, non-vortex beam. This can be better understood by comparing intensities at the focus in Equations (7) and (18). From (7), the transverse intensity, $I_{0,0}^2 + I_{2,2}^2$, is seen to have a maximum on the optical axis, while the longitudinal intensity, $2I_{1,1}^2$, is shaped as a ring with the on-axis intensity null. Therefore, the contribution to the central region of the focal spot from the longitudinal intensity is smaller when compared with the transverse intensity, with a flat top not observed in the focal spot in Figure 3. Vice versa, Equation (18) suggests that the transverse intensity, $I_{0,1}^2 + I_{2,1}^2$, is shaped as a ring with the on-axis intensity null, whereas the longitudinal intensity, $2I_{1,0}^2$, has an on-axis maximum, with the contributions from the both components being near the same. As a result, the focal spot has a flatter top (Figure 10).

Let us also consider the behavior of the polarization at the focus. Figure 11c shows the distributions of the third component of the normalized Stokes vector at the focus of a flat diffractive lens with $NA = 0.95$.

From Figure 11c, it can be seen that, only when focusing circularly polarized light beams, regions with the alternating directions of the polarization vector rotation are observed at the focus.

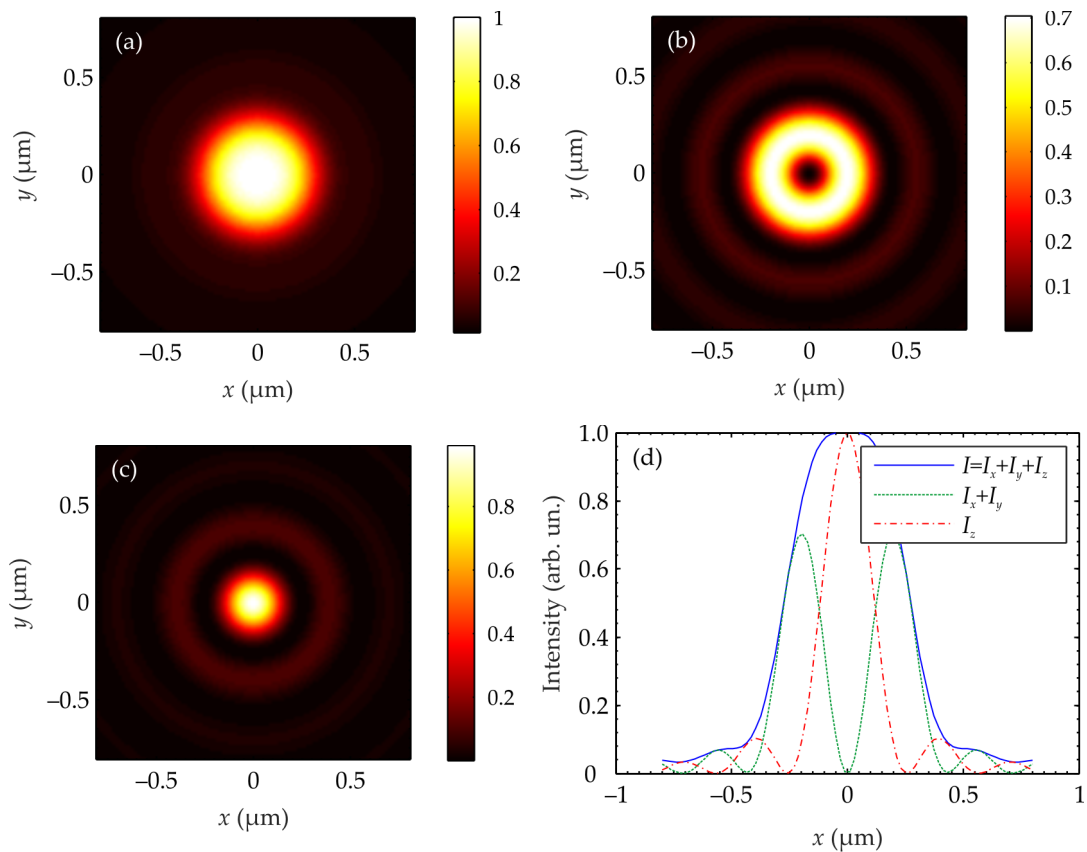


Figure 10. Flat-top focus when focusing an optical vortex ($m = -1$) with a flat diffractive lens with a numerical aperture of $\text{NA} = 0.93$. Distributions of intensity at the focus (a) and intensity components I_r (b) and I_z (c). The intensity profile along the x -axis (d).

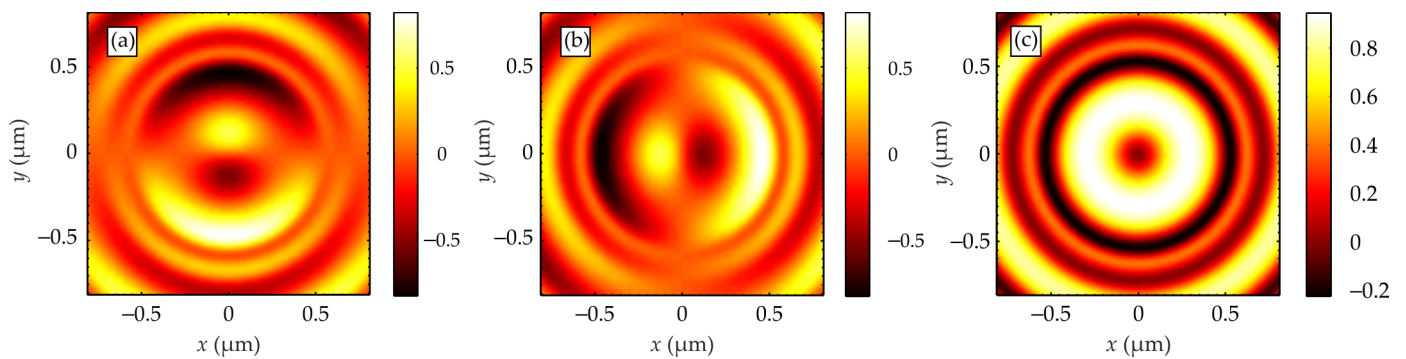


Figure 11. Distribution of the three components of the normalized Stokes vector S_1 (a), S_2 (b), S_3 (c) in the plane of focus when an optical vortex ($m = -1$) is focused by a flat diffractive lens with $\text{NA} = 0.95$.

4. Conclusions

In this paper, using the Richards–Wolf formalism, the focusing of light with circular polarization with flat diffractive lenses was considered. It has been shown that, as the numerical aperture of the lens increases, the size of the focal spot first decreases and then begins to grow. The minimum focal spot is observed at $\text{NA} = 0.96$ ($\text{FWHM} = 0.55 \lambda$). With a further increase in the numerical aperture of the lens, the growth of the longitudinal component leads to an increase in the size of the focal spot. When a flat diffractive lens is replaced by an aplanatic lens, the size of the focal spot decreases monotonically as the numerical aperture of the lens increases.

This phenomenon may be ascribed to the fact that diffractive and aplanatic lenses have different apodization functions. In a planar diffractive lens, the apodization function entering the Debye integral (1) is given by $T(\theta) = \cos^{-3/2}\theta$ and increases with increasing angle θ from 0 to $\pi/2$. Because of this, at large NA ≈ 1 , the focal spot size becomes larger. At the same time, in a conventional refractive ideal spherical lens, the apodization function is given by $T(\theta) = \cos^{1/2}\theta$ and decreases with an increasing angle θ from 0 to $\pi/2$. Therefore, with increasing NA, the size of the focal spot decreases monotonically.

Interestingly, the most homogeneous intensity distribution in the focal plane has been found to be attained when focusing an optical vortex with a planar diffractive lens with NA = 0.93 (Figure 10).

We have also revealed that, at the focus of a circularly polarized optical beam, different-radius circular regions centered on the optical axis are formed with alternating directions of the polarization vector rotation (clockwise and anticlockwise). Such a radius-dependent separation of oppositely directed ‘spins’ is a manifestation of the radial spin Hall effect at the focus.

Potential application areas are as follows: a flat-top focus (Figure 10) can find uses in microscopy for producing a homogeneous visual field, whereas the radial spin Hall effect (Figures 7 and 11) can be used to set absorbing microparticles into the opposite-handed rotation (clockwise and anticlockwise) by partially transferring to them the spin angular momentum of light.

Author Contributions: Conceptualization, V.V.K.; methodology, S.S.S. and V.V.K.; software, S.S.S.; validation, S.S.S. and V.V.K.; formal analysis, V.V.K.; investigation, S.S.S., V.D.Z. and V.V.K.; resources, S.S.S.; data curation, V.V.K.; writing—original draft preparation, S.S.S. and V.D.Z.; writing—review and editing, V.V.K.; visualization, S.S.S.; supervision, V.V.K.; project administration, S.S.S.; funding acquisition, S.S.S. All authors have read and agreed to the published version of the manuscript.

Funding: This research was funded by Russian Science Foundation, grant number 22-22-00265.

Institutional Review Board Statement: Not applicable.

Informed Consent Statement: Not applicable.

Data Availability Statement: Not applicable.

Conflicts of Interest: The authors declare no conflict of interest.

References

1. Man, Z.; Dou, X.; Urbach, H.P. The evolutions of spin density and energy flux of strongly focused standard full Poincaré beams. *Opt. Commun.* **2020**, *458*, 124790. [[CrossRef](#)]
2. Man, Z.; Bai, Z.; Zhang, S.; Li, X.; Li, J.; Ge, X.; Zhang, Y.; Fu, S. Redistributing the energy flow of a tightly focused radially polarized optical field by designing phase masks. *Opt. Express* **2018**, *26*, 23935. [[CrossRef](#)] [[PubMed](#)]
3. Gao, X.-Z.; Pan, Y.; Zhang, G.-L.; Zhao, M.-D.; Ren, Z.-C.; Tu, C.-G.; Li, Y.-N.; Wang, H.-T. Redistributing the energy flow of tightly focused ellipticity-variant vector optical fields. *Photonics Res.* **2017**, *5*, 640. [[CrossRef](#)]
4. Jiao, X.; Liu, S.; Wang, Q.; Gan, X.; Li, P.; Zhao, J. Redistributing energy flow and polarization of a focused azimuthally polarized beam with rotationally symmetric sector-shaped obstacles. *Opt. Lett.* **2012**, *37*, 1041. [[CrossRef](#)] [[PubMed](#)]
5. Richards, B.; Wolf, E. Electromagnetic Diffraction in Optical Systems. II. Structure of the Image Field in an Aplanatic System. *Proc. R. Soc. A Math. Phys. Eng. Sci.* **1959**, *253*, 358–379.
6. Stafeev, S.S.; Nalimov, A.G.; Kovalev, A.A.; Zaitsev, V.D.; Kotlyar, V.V. Circular Polarization near the Tight Focus of Linearly Polarized Light. *Photonics* **2022**, *9*, 196. [[CrossRef](#)]
7. Bauer, T.; Banzer, P.; Karimi, E.; Orlov, S.; Rubano, A.; Marrucci, L.; Santamato, E.; Boyd, R.W.; Leuchs, G. Observation of optical polarization Möbius strips. *Science* **2015**, *347*, 964–966. [[CrossRef](#)]
8. Wang, H.; Shi, L.; Lukyanchuk, B.; Sheppard, C.; Chong, C.T. Creation of a needle of longitudinally polarized light in vacuum using binary optics. *Nat. Photonics* **2008**, *2*, 501–505. [[CrossRef](#)]
9. Dorn, R.; Quabis, S.; Leuchs, G. Sharper Focus for a Radially Polarized Light Beam. *Phys. Rev. Lett.* **2003**, *91*, 233901. [[CrossRef](#)]
10. Grosjean, T.; Gauthier, I. Longitudinally polarized electric and magnetic optical nano-needles of ultra high lengths. *Opt. Commun.* **2013**, *294*, 333–337. [[CrossRef](#)]
11. Wang, X.; Zhu, B.; Dong, Y.; Wang, S.; Zhu, Z.; Bo, F.; Li, X. Generation of equilateral-polygon-like flat-top focus by tightly focusing radially polarized beams superposed with off-axis vortex arrays. *Opt. Express* **2017**, *25*, 26844–26852. [[CrossRef](#)] [[PubMed](#)]

12. Ping, C.; Liang, C.; Wang, F.; Cai, Y. Radially polarized multi-Gaussian Schell-model beam and its tight focusing properties. *Opt. Express* **2017**, *25*, 32475–32490. [[CrossRef](#)]
13. Chen, H.; Tripathi, S.; Toussaint, K.C. Demonstration of flat-top focusing under radial polarization illumination. *Opt. Lett.* **2014**, *39*, 834–837. [[CrossRef](#)] [[PubMed](#)]
14. Kasinski, J.J.; Burnham, R.L. Near-diffraction-limited laser beam shaping with diamond-turned aspheric optics. *Opt. Lett.* **1997**, *22*, 1062. [[CrossRef](#)]
15. Li, Y. Light beams with flat-topped profiles. *Opt. Lett.* **2002**, *27*, 1007. [[CrossRef](#)]
16. Eyyuboglu, H.T.; Arpali, Ç.; Baykal, Y.K. Flat topped beams and their characteristics in turbulent media. *Opt. Express* **2006**, *14*, 4196. [[CrossRef](#)]
17. Kotlyar, V.V.; Nalimov, A.G.; Stafeev, S.S. Exploiting the circular polarization of light to obtain a spiral energy flow at the subwavelength focus. *J. Opt. Soc. Am. B* **2019**, *36*, 2850–2855. [[CrossRef](#)]
18. Stafeev, S.S.; Zaitsev, V.D.; Kotlyar, V.V. Circular polarization before and after the sharp focus for linearly polarized light. *Comput. Opt.* **2022**, *46*, 381–387. [[CrossRef](#)]
19. Davidson, N.; Bokor, N. High-numerical-aperture focusing of radially polarized doughnut beams with a parabolic mirror and a flat diffractive lens. *Opt. Lett.* **2004**, *29*, 1318–1320. [[CrossRef](#)]
20. Stafeev, S.S.; Zaicev, V.D. A minimal subwavelength focal spot for the energy flux. *Comput. Opt.* **2021**, *45*, 685–691. [[CrossRef](#)]
21. Stafeev, S.S.; Nalimov, A.G. Longitudinal component of the Poynting vector of a tightly focused optical vortex with circular polarization. *Comput. Opt.* **2018**, *42*, 190–196. [[CrossRef](#)]

Disclaimer/Publisher’s Note: The statements, opinions and data contained in all publications are solely those of the individual author(s) and contributor(s) and not of MDPI and/or the editor(s). MDPI and/or the editor(s) disclaim responsibility for any injury to people or property resulting from any ideas, methods, instructions or products referred to in the content.